






Cite this: *Mater. Adv.*, 2025,  
6, 4857

# Improving the adsorption efficiency of a low-cost natural adsorbent for the removal of an organic pollutant: optimization and mechanism study†

Yahia Saghir, \* Ayoub Chaoui, Salaheddine Farsad,  Aboubakr Ben Hamou,   
Asma Amjlef,  Mohamed Benafqir,  Nouredine El Alem and Mohamed Ez-zahery

Water scarcity and contamination due to organic pollutants (dyes, antibiotics, pesticides, etc.) have constituted a major problem for humanity in recent decades. In this context, the present work explores the adsorption capacity of modified clay as an adsorbent for the removal of crystal violet (CV) dye from aqueous solutions. The modification combines the basic activation and thermal treatment processes at various temperatures (350 °C to 750 °C). The adsorption performance of the chosen adsorbent was systematically evaluated through batch adsorption experiments using the RSM-Doehlert methodology. The effect of different factors, namely, the adsorbent dose (AD), contact time (CT), and initial CV concentration (IC), at natural pH (pH = 5.29) and room temperature ( $T = 23 \pm 2$  °C) on the adsorption capacity of CV was evaluated. The significance of the model was assessed using analysis of variance (ANOVA). Results indicate that the optimum conditions for maximum removal are as follows: AD = 0.5 g L<sup>-1</sup>, CT = 95 min, and IC = 118.8 mg L<sup>-1</sup>. Kinetics and isotherms suggest that the experimental data are better described by the nonlinear pseudo-second-order (PSO) model and nonlinear Langmuir isotherm. The adsorption capacity obtained based on the Langmuir isotherm was 1199.93 mg g<sup>-1</sup>. Moreover, the adsorption process is spontaneous and exothermic, as determined through the thermodynamic study. The proposed adsorption mechanism involves hydrogen bonding, n- $\pi$  interactions, and cationic substitutions in the interfoliar space of the AC-750 °C adsorbent. This approach offers a promising pathway for incorporating sorbents derived from natural resources, such as clays, into advanced water treatment engineering practices, achieving high adsorption capacity for various organic pollutants, including cefazolin and tetracycline.

Received 20th March 2025,  
Accepted 2nd June 2025

DOI: 10.1039/d5ma00253b

rsc.li/materials-advances

## 1. Introduction

Water is an essential resource for human survival. It comes from various sources, including lakes, ponds, rivers, and groundwater. However, the quality of this precious resource is deteriorated by pollution.<sup>1–3</sup> The leading causes of this problem are related to industrial, commercial, and agricultural activities. Industrial activities generate a significant amount of organic and inorganic pollutants.<sup>4,5</sup> Among the diverse organic pollutants generated by industrial activities, dyes are recognized as toxic substances that pose significant risks to ecosystems and human health.<sup>4</sup> Crystal violet (CV) is a cationic dye well known for its harmful effects on human health as a potent mitotic toxin and carcinogen and is linked to tumor

development in certain fish species.<sup>1</sup> The international standard for dyeing effluent discharge stipulates that, for CV dyeing, the maximum color concentration must not exceed 1 mg L<sup>-1</sup>, and the effluent must not contain any harmful chemicals.<sup>6</sup>

From an environmental perspective, the remediation of water contaminated with organic pollutants has become a major environmental challenge, as organic pollutants contaminate groundwater and surface water through leaching and runoff.<sup>7–9</sup> Several methods have been employed to remove harmful pollutants from water to tackle this challenge. These methods encompass chemical, physical, and biological treatments, including ion exchange, coagulation, membrane filtration, precipitation, advanced oxidation, and reverse osmosis processes.<sup>1,2,4</sup> The application of these techniques can be limited by many drawbacks, such as effectiveness, cost, and energy consumption.<sup>1</sup> Lately, the adsorption process has received significant attention owing to its operational simplicity, inexpensiveness, and higher efficiency compared with

Laboratory of Materials and Environment, Ibn Zohr University, Agadir, 8000, Morocco. E-mail: yahya.saghir.edu@gmail.com

† Electronic supplementary information (ESI) available. See DOI: <https://doi.org/10.1039/d5ma00253b>

conventional water treatment techniques.<sup>4</sup> The application of this technique is based on selecting a suitable adsorbent.<sup>10</sup> This choice depends on different criteria, including availability, abundance, low cost, and environmental friendliness.<sup>4,5</sup> For this reason, an alternative adsorbent has been widely used in the current research due to its high adsorption capacity.<sup>11</sup> Clays are characterized by their structure, high specific surface area, and cation exchange capacity (CEC).<sup>2,11</sup> These properties confer excellent adsorption efficiency on clays towards various pollutants.<sup>12</sup> Some pollutants have a low adsorption capacity on natural clays, requiring additional treatment, such as acid and basic activation or other modification techniques to increase their adsorption capacity.<sup>13–16</sup> Among these processes, basic activation and thermal treatment have shown better adsorption capacity for pollutants.<sup>17</sup> The basic activation process consists of ion exchange in the interlayer of clays, such as the exchange of  $\text{Ca}^{2+}$  ions by  $\text{Na}^+$  ions when treating the clays with sodium carbonate ( $\text{Na}_2\text{CO}_3$ ) solution, which can contribute to an increase in CEC and adsorption efficiency of the clay.<sup>18</sup> In comparison, the thermal treatment is a simple and inexpensive process.<sup>19</sup> In this treatment, the clay is heated to a specific temperature, which can affect its structural and textural properties due to dehydroxylation and dehydration processes.<sup>19–21</sup> The combination of basic activation and thermal treatment improves the morphological and cation exchange capacity of clays, thereby increasing the adsorption capacity.<sup>17</sup> In this context, several studies have examined the influence of a combination of  $\text{Na}_2\text{CO}_3$  activation and thermal treatment on the adsorption capacity of bentonite clay towards heavy metals. El Ouardi *et al.*<sup>3</sup> found that the adsorption capacity increased from 5.6 to 10.7  $\text{mg g}^{-1}$  and 6 to 7.1  $\text{mg g}^{-1}$  for nickel and silver, respectively, after  $\text{Na}_2\text{CO}_3$  activation and calcination at 450 °C. Similar trends have been demonstrated for cadmium removal through the adsorption process. The results show that cadmium adsorption capacity increased from 43.10 to 61.81  $\text{mg g}^{-1}$  after  $\text{Na}_2\text{CO}_3$  activation and thermal treatment at 350 °C.<sup>20</sup> To our knowledge, no scientific reports are available on optimizing the CV dye adsorption process on natural muscovite-type clays subjected to  $\text{Na}_2\text{CO}_3$  activation and heat treatment using response surface methodology (RSM).

This study focuses on obtaining a high adsorption capacity of CV dye through the valorization of natural clay (NC) as an adsorbent. For this purpose, the NC was first activated with  $\text{Na}_2\text{CO}_3$ , followed by thermal treatment at various temperatures (350 to 750 °C). The physicochemical, mineralogical, microstructural, and thermal properties of natural and modified clay were evaluated. A Doehlert matrix was employed within the RSM framework using Nemrodw software. This analysis enabled the determination of optimum conditions for maximal CV dye adsorption efficiency. Furthermore, adsorption kinetics, isotherms, thermodynamic parameters, and adsorption mechanism were also studied.

## 2. Materials and methods

### 2.1. Adsorbent and adsorbate preparation

The NC used in this study was extracted from the Agadir region of Morocco and employed as an adsorbent support. It was subjected to mechanical preparation, chemical, and thermal treatments as per earlier reports. The NC was initially ground in a porcelain mortar and sieved to obtain a fine powder with a diameter of less than 50  $\mu\text{m}$ . For basic activation, 30 g of sieved clay and 1.5 g of sodium carbonate were stirred continuously for 1 h at 75 °C in 300 ml of distilled water.<sup>22</sup> After stirring, the obtained solution was filtered and repeatedly washed with distilled water, and then the activated clay (AC) was transferred to an oven at 70 °C until completely dehydrated. The resultant material was ground and subjected to thermal treatment in a muffle furnace at various temperatures (350 to 750 °C) for 4 h with a heating rate of 5 °C  $\text{min}^{-1}$ ; the resulting treated clays were designated as follows (AC-350 °C, AC-450 °C, AC-550 °C, AC-650 °C, and AC-750 °C), which are all grouped under the term modified clays (MC), as mentioned in Fig. 1. Finally, the samples were preserved and stored in glass bottles. Fig. 1 summarizes the preparation process of modified clays.

The adsorbate used in this study is the CV dye. The main characteristics of this dye are summarized in Table S1 (ESI†).<sup>1</sup> The stock solution is prepared by dissolving 1 g of the CV dye

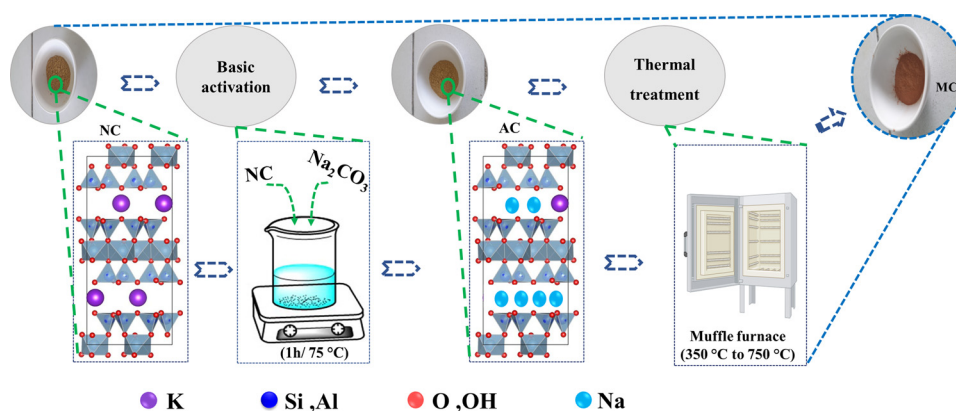


Fig. 1 Preparation of modified clays (MCs).



powder in 1 L of distilled water and then diluting to the specified concentrations.

## 2.2. Characterization methods

Crystalline phases present in natural and modified clays were characterized using X-ray diffraction (XRD) analysis on a Bruker D8 Advance Twin powder diffractometer using Cu-K $\alpha$  radiation ( $\lambda(\text{K}\alpha\text{Cu}) = 1.5418 \text{ \AA}$ ) operating in the range of  $10^\circ$  and  $70^\circ$ . The microstructural analysis of the clay was performed using a JEOL JSM IT-100 scanning electron microscope (SEM) equipped with energy-dispersive X-ray spectrometry to determine the elemental chemical composition. In addition, Fourier transform infrared spectroscopy (FTIR) was also be used to provide information about the main f groups of natural and modified clays. Spectra were obtained over  $400 \text{ cm}^{-1}$  to  $4000 \text{ cm}^{-1}$  using a SHIMADZU IRAffinity-1S at a resolution of  $16 \text{ cm}^{-1}$ . The point of zero charge ( $\text{pH}_{\text{pzc}}$ ) was determined as described by Imgharn *et al.*<sup>23</sup>. Moreover,  $\text{N}_2$  sorption experiments at 77 K were conducted using a TriStar II Plus Surface Characterization Analyzer (Micromeritics), covering relative pressures up to 1 bar. The cryogenic temperature for  $\text{N}_2$  sorption was controlled through a liquid nitrogen bath at 77 K. Specific surface area was determined using the Brunauer–Emmett–Teller (BET) model to determine the  $\text{N}_2$  adsorption isotherms collected at 77 K. Thermal properties were investigated by thermogravimetric analysis (TGA) in the temperature range of 25 and  $900^\circ\text{C}$  using an SDTQ600 TA instrument with a controlled heating rate of  $10^\circ\text{C min}^{-1}$  under a flow of air.

## 2.3. Adsorption experiments and regeneration process

The efficiency of AC-750  $^\circ\text{C}$  for the adsorption of CV was tested in a batch system by changing various parameters, including the adsorbent dose (AD,  $0.4\text{--}2 \text{ g L}^{-1}$ ), contact time (CT,  $10\text{--}180 \text{ min}$ ), and initial CV concentration (IC,  $20\text{--}150 \text{ mg L}^{-1}$ ) based on the experiments generated from Doehlert matrix using Nemrodw software. The effect of pH was also examined in a range from 2 to 12. The entire adsorption process was performed by adding a specific amount of AC-750  $^\circ\text{C}$  to 25 ml of CV dye. This mixture was then placed on a magnetic stirrer regulated at 200 rpm. At the end of the adsorption experiments, a required volume of the solution was drawn off and filtered with a  $0.45 \mu\text{m}$  syringe filter. The residual concentration of the CV dye was determined using a UV-visible spectrophotometer (6705 UV-visible JENWAY) at  $\lambda = 590 \text{ nm}$ . The CV dye adsorption capacity ( $q_e$ ) and its percentage removal were determined from the equations below:<sup>24</sup>

$$q_e = \frac{C_0 - C_e}{m} V \text{ (mg g}^{-1}\text{)} \quad (1)$$

$$R = \frac{C_0 - C_e}{C_0} \times 100(\%) \quad (2)$$

The initial and equilibrium concentrations of the CV solution are defined by ( $C_0$ ,  $\text{mg L}^{-1}$ ) and ( $C_e$ ,  $\text{mg L}^{-1}$ ), respectively,  $V$  (L) represents the volume of the CV dye solution, and  $m$  (g) denotes the amount of AC-750  $^\circ\text{C}$  employed.

After the adsorption experiments, the regeneration process is necessary for the subsequent use of the adsorbent. The CV-loaded AC-750  $^\circ\text{C}$  (AC-750  $^\circ\text{C@CV}$ ) was introduced into a beaker containing ethanol solvent at room temperature for 4 h. After the soaking time, the recovered AC-750  $^\circ\text{C}$  adsorbent was cleaned with distilled water and subjected to heat treatment at  $750^\circ\text{C}$ . It was then reapplied for CV dye adsorption-desorption and repeated thrice under the same conditions.

## 2.4. Modeling and design of experiments

According to previous studies,<sup>25,26</sup> Doehlert matrix was selected as the experimental design. Using a second-degree polynomial model, the adsorption capacity of CV onto AC-750  $^\circ\text{C}$  (response) was assessed with respect to three parameters. The objective was to obtain the best performance in the parameters considered.

The effect of different parameters (AD, CT, and IC) on the sorption capacity of the CV dye onto AC-750  $^\circ\text{C}$  was evaluated by adopting the following model (eqn (3)):

$$Y = b_0 + \sum_{i=1}^k b_i X_i + \sum_{i=1}^k b_{ii} X_i^2 + \sum_{i=1}^{k-1} \sum_{j=i+1}^k b_{ij} X_i X_j \quad (3)$$

$X_{i(i \in [1-3])}$  presents the coded variables corresponding to the factors considered, AD, CT, and IC, respectively. The coded variables are obtained from the following mathematical equations.

$$X_1 = \frac{(\text{AD} - \text{AD}_0)}{\Delta\text{AD}} \quad (4)$$

$$X_2 = \frac{(\text{CT} - \text{CT}_0)}{\Delta\text{CT}} \quad (5)$$

$$X_3 = \frac{(\text{IC} - \text{IC}_0)}{\Delta\text{IC}} \quad (6)$$

$Y_1$  represents the response, and  $b_0$  is a constant value.  $b_1$ ,  $b_2$ , and  $b_3$  reflect the effects of the adsorbent dose, contact time, and CV initial concentration, respectively.  $b_{ii}$  and  $b_{ij}$  are attributed to the curve shape parameter and weight of the interactive impact between the factors  $i$  and  $j$ , respectively.

$\text{AD}_0$ ,  $\text{CT}_0$ , and  $\text{IC}_0$  represent the adsorbent dose, contact time, and initial CV concentration at the null point, respectively ( $\text{AD}_0 = 1.2 \text{ g L}^{-1}$ ,  $\text{CT}_0 = 95 \text{ min}$ , and  $\text{IC}_0 = 85 \text{ mg L}^{-1}$ ).  $\Delta\text{AD}$ ,  $\Delta\text{CT}$ , and  $\Delta\text{IC}$  are the variation steps of the factors ( $\Delta\text{AD} = 0.5 \text{ g L}^{-1}$ ,  $\Delta\text{CT} = 95 \text{ min}$ , and  $\Delta\text{IC} = 85 \text{ mol L}^{-1}$ ). Nemrodw software was used to determine the values of each of the above-mentioned factors.<sup>27</sup> To assess the experimental error, the experience at the center was repeated three times. An analysis of variance (ANOVA) was applied to confirm the accuracy of the chosen model. The results are given in Table 2.<sup>28</sup>

## 2.5. Kinetics study

This study aims to assess the influence of time on the adsorption performance of the CV dye by the AC-750  $^\circ\text{C}$  adsorbent. The pseudo-first-order (PSF), pseudo-second-order (PSO), intra-particle diffusion (IPD), and Elovich models were applied to the



experimental data. The main equations of each model are given in Table S2 (ESI†).<sup>29</sup>

## 2.6. Isotherm's modeling

Isotherm experiments were conducted under optimized conditions, employing 25 mL solutions with initial CV concentrations varying from 10 to 900 mg L<sup>-1</sup>. All experiments were agitated at 200 rpm and maintained at ambient temperature for 95 min to establish equilibrium. The resulting adsorption data for CV on AC-750 °C were analyzed using the classical isotherm models of Langmuir, Freundlich, and Temkin. The isotherm equations in their linear and nonlinear forms are summarized in Table S3 (ESI†).<sup>29</sup>

# 3. Results and discussion

## 3.1 Characterization of NC and MC

The XRD analysis of NC and MC is shown in Fig. 2(a). The results show that the natural clay consists of muscovite (M) and hematite (H), along with impurities of calcite (C) and quartz (Q). Upon the modification process, the intensity of the muscovite peaks at  $2\theta = 18.10^\circ$  and  $35.14^\circ$  decreased, confirming a molecular spacing change resulting from the exchange of K<sup>+</sup> ions by Na<sup>+</sup> ions after basic activation and the release of almost all the water

molecules following the heat treatment in the 350–550 °C range.<sup>18,19,30</sup> In addition, after the heat treatment at 650 °C and 750 °C, the two similar peaks of muscovite increased in intensity, indicating an expansion of the unit-cell parameters of muscovite.<sup>31</sup> It must also be noted that the peak located at  $2\theta = 35.14^\circ$  was shifted to lower angles upon thermal treatment at 650 °C due to the dehydroxylation of muscovite.<sup>32</sup> As already known, the dehydroxylation of muscovite is accelerated and completed between 640 °C and 820 °C.<sup>33</sup> However, as the dehydroxylation process progresses, the loss of hydroxyl groups occurs non-uniformly, and the remaining hydroxyl groups exhibit an increased affinity for aluminum cations in an unusual quintuple coordination, opposing and delaying the overall process of a hydroxyl group departure.<sup>34</sup> Furthermore, it can be seen that the decomposition of the calcite phase begins at a temperature of 650 °C. Indeed, calcite decomposition starts at 600 °C and is entirely completed at 850 °C.<sup>35</sup> Moreover, the quartz phase was observed in the MC, confirming their resistance to the modification process.

Fig. 2(b) shows the FTIR spectra of natural and modified clays. The spectrum reveals the presence of a variety of bands. The bands at 3630 cm<sup>-1</sup> and 3427 cm<sup>-1</sup> are associated with the stretching vibrations of structural OH groups and water stretching vibrations, respectively.<sup>36,37</sup> The peak observed at 1010 cm<sup>-1</sup> is assigned to the Si-O stretching vibrations.<sup>38</sup> The

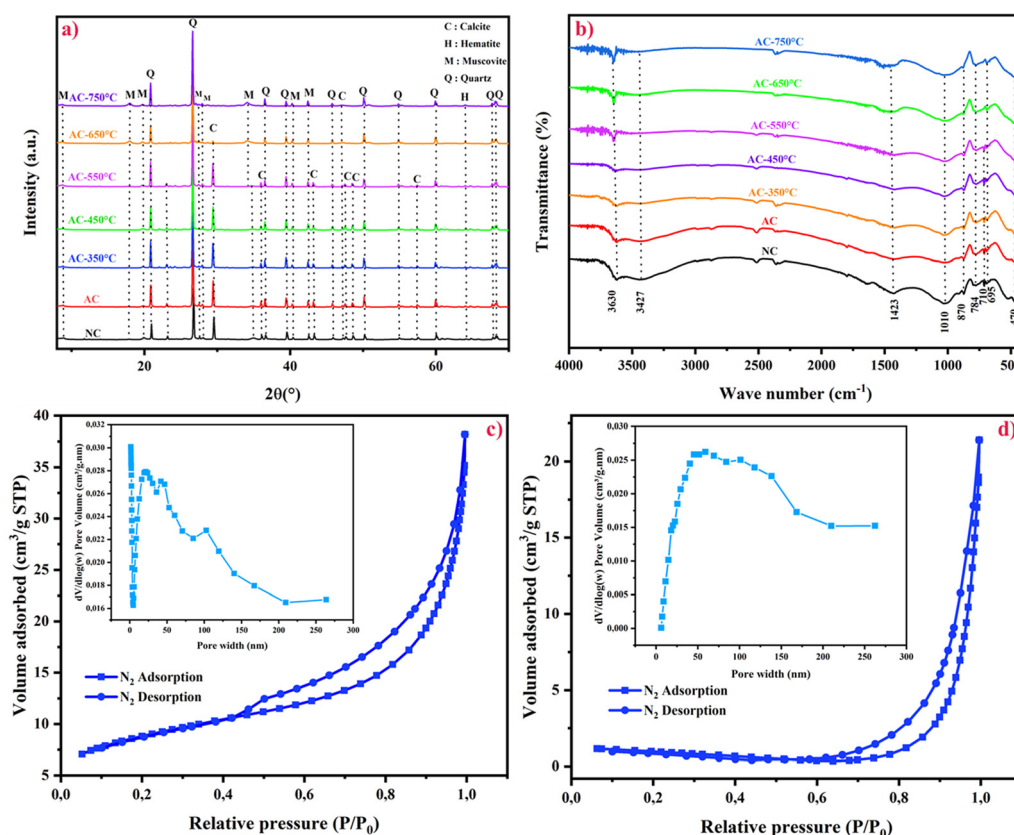


Fig. 2 Mineralogical composition (a) and infrared spectra (b) of natural and modified clays, and nitrogen isotherm adsorption–desorption curves of NC (c) and AC-750 °C (d) at 77 K.





peak located at  $870\text{ cm}^{-1}$  corresponds to the stretching of Al–Al–OH groups.<sup>39</sup> Other bands that appeared at  $784\text{ cm}^{-1}$  and  $695\text{ cm}^{-1}$  are attributed to the deformation vibrations of Si–O–Si.<sup>37</sup> The band appearing at  $470\text{ cm}^{-1}$  is associated with the deformation vibrations of Si–O–Al.<sup>40</sup> The bands located at  $1423\text{ cm}^{-1}$  and  $710\text{ cm}^{-1}$  represent the valence vibrations of C=O in calcite.<sup>41</sup> Post-modification, the intensity of the two bands related to water molecules (OH) and C=O located at  $1423\text{ cm}^{-1}$  is significantly reduced. The increased intensity of the OH stretching band at  $3630\text{ cm}^{-1}$  suggests a structural modification and indicates that the dehydroxylation process is non-homogeneous.<sup>42,43</sup> After basic activation, the intensity of the band associated with the Si–O group decreased as a result of the change in the sodium content between NC and AC.<sup>20</sup> In addition, the band located at  $710\text{ cm}^{-1}$  disappeared after thermal treatment at  $650\text{ }^{\circ}\text{C}$ , confirming the decomposition of calcite.

Fig. 2(c) and (d) shows the  $\text{N}_2$  adsorption–desorption isotherms for both the NC and AC- $750\text{ }^{\circ}\text{C}$  samples. According to the IUPAC adsorption isotherm classification, the NC and AC- $750\text{ }^{\circ}\text{C}$  samples followed the type IV isotherm, revealing mesopores in these materials with pore sizes of the order of 2–50 nm.<sup>20,44</sup> For the hysteresis type, NC and AC- $750\text{ }^{\circ}\text{C}$  samples exhibit a type  $\text{H}_3$  hysteresis loop, which indicates a structure with plate-like particle aggregates giving rise to lamellar pores.<sup>45</sup> Furthermore, after the modification process, the results reveal a change in surface area and total pore volume. The latter shows a decline from  $0.0031$  to  $2.6000\text{ cm}^3\text{ g}^{-1}$  for NC and AC- $750\text{ }^{\circ}\text{C}$ , respectively. Similar results were obtained for the BET surface area, which was significantly reduced from  $30.4100$  to  $2.6000\text{ m}^2\text{ g}^{-1}$ . These results indicate that heat treatment promotes grain growth, leading to a reduction in surface area.<sup>20</sup>

The morphology of NC and MC was analyzed using SEM. The NC images (Fig. 3(a)) show that the particle shapes are

irregular, with grain sizes ranging from 10 to  $200\text{ }\mu\text{m}$ . After basic activation, the surface of the AC (Fig. 3(b)) becomes smoother. The SEM images of AC- $750\text{ }^{\circ}\text{C}$  (Fig. 3(c)) exhibit similar morphologies to the NC but appear more dispersed with an increase in grain size particles due to the thermal treatment, demonstrating that the modification process did not alter the clay's fundamental crystalline structure.<sup>3,32</sup> This morphology suggest that the modified clay could provide abundant adsorption active sites, which can be advantageous for the adsorption.

The qualitative EDS analysis revealed that all samples contained mainly the elements silica (Si), aluminum (Al), oxygen (O), calcium (Ca), potassium (K), and magnesium (Mg), as shown in Table S4 (ESI†). In addition, a low sodium (Na) content was observed in AC and AC- $750\text{ }^{\circ}\text{C}$ , resulting in ion exchange upon  $\text{Na}_2\text{CO}_3$  activation.

The thermal behavior of the NC sample was analyzed using TGA, as depicted in Fig. 3(d). The TGA curve highlights three main weight losses. The first loss ( $-1.8\%$ ), between  $20$  and  $350\text{ }^{\circ}\text{C}$ , reflects the elimination of both physically adsorbed water and adsorbed surface water.<sup>37,46</sup> The second loss, of the order of  $-2\%$ , occurs from  $350\text{ }^{\circ}\text{C}$  up to  $620\text{ }^{\circ}\text{C}$ , which is caused by the degradation of organic matter and the decomposition of calcium carbonate.<sup>47,48</sup> Above  $620\text{ }^{\circ}\text{C}$ , the weight loss reaches its maximum ( $-8\%$ ), which is attributed to the dehydroxylation process resulting from the release of structural OH groups from the clay structure.<sup>46</sup> As shown by both XRD and FTIR analyses, thermal treatment at  $750\text{ }^{\circ}\text{C}$  induces partial dehydroxylation, leading to expandable muscovite. The latter allows CV dye molecules to intercalate in the interlayer space, thus increasing the adsorption capacity. Neisser-Deiters, Axel, *et al.*<sup>49</sup> have reported that heat treatment can increase lattice parameters, which in turn leads to an increase in unit cell volume, resulting in improved water absorption capacity. Jia Feifei *et al.*<sup>50</sup> have also demonstrated that the expanded

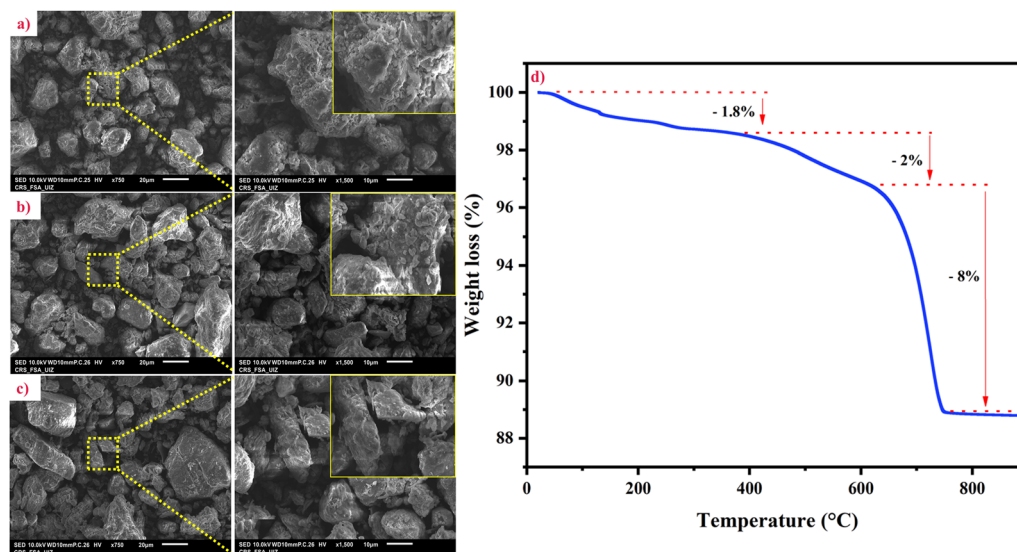


Fig. 3 SEM images of NC (a), AC (b), and AC- $750\text{ }^{\circ}\text{C}$  (c); TGA (d) of NC.



muscovite has important potential applications in the adsorption and filling industries.

### 3.2. Adsorption experiments

**3.2.1. Effect of the modification process.** The modification process of NC involves the basic activation and the combination of basic activation and thermal treatment. The results show that the adsorption capacity is regularly linked to the type of modification process. Adsorption experiments were undertaken to test the behavior of raw and modified clays in the removal of the CV dye under the same conditions: an AD of  $1 \text{ g L}^{-1}$ , IC of  $100 \text{ mg L}^{-1}$ , CT of 180 min at  $\text{pH} = 5.29$ , and room temperature for all samples.

Fig. 4 illustrates the evolution of the adsorption capacity of the CV dye according to the clay type. The results highlighted a significant change in the adsorption capacity of the CV dye. The adsorption capacity was reduced from  $49.35 \text{ mg g}^{-1}$  for NC to  $38.61 \text{ mg g}^{-1}$  for AC after  $\text{Na}_2\text{CO}_3$  activation, confirming that  $\text{K}^+$  was successfully substituted by  $\text{Na}^+$ , leading to a reduction in the layer spacing.<sup>30,51</sup>  $\text{Na}_2\text{CO}_3$  activation was used to enhance the physicochemical properties of NC. However, the adsorption capacity is reduced in this case. Similar results were found in a previous study conducted by Eniola *et al.*<sup>20</sup> for cadmium adsorption on activated bentonite clay, which demonstrated that the adsorption capacity of bentonite clay was reduced from  $43.10$  to  $30.92 \text{ mg g}^{-1}$  after  $\text{Na}_2\text{CO}_3$  activation. These results suggest that not all modification processes necessarily lead to an improvement in adsorption performance. Under heat treatment, the adsorption capacity of NC continues to decrease, reaching a minimum value of  $32.27 \text{ mg g}^{-1}$  at  $550^\circ\text{C}$  due to the removal of superficial and interlaminar water, leading to a reduction in basal space and surface area without showing any changes in the crystalline structure. However, after the heat treatment at  $650^\circ\text{C}$  and  $750^\circ\text{C}$ , the adsorption capacity of the CV dye improved to reach the highest value ( $100 \text{ mg g}^{-1}$ ) for AC- $750^\circ\text{C}$ . According to a previous study, the decontamination of polluted water is more successfully achieved by combining two modification methods.<sup>52</sup> These results were consistent with

X-ray diffraction, FTIR, and TG analyses. As a result, AC- $750^\circ\text{C}$  was chosen for a more in-depth study of CV dye adsorption to identify the specific factors contributing to its enhanced adsorption capacity.

**3.2.2. Effect of pH.** The pH factor is considered a key factor in elucidating the adsorption mechanism between CV dye molecules and AC- $750^\circ\text{C}$ . It is well known for its effect on the ionization state of the adsorbate and the surface charge of the adsorbent.<sup>53,54</sup> To achieve the maximum adsorption capacity, the optimum pH was identified by adding  $25 \text{ mg}$  of the AC- $750^\circ\text{C}$  adsorbent to  $25 \text{ ml}$  of an initial concentration of  $50 \text{ mg L}^{-1}$  CV dye. Irrespective of the pH being basic or acidic, the results revealed a greater affinity between the CV dye molecules and AC- $750^\circ\text{C}$  (Fig. 5). The ideal pH ( $5.29$ ), corresponding to the maximum adsorption capacity ( $50 \text{ mg g}^{-1}$ ), was used for the rest of the adsorption studies.

**3.2.3. Optimization of variable RSM methodology.** To evaluate and optimize the CV dye adsorption capacity as a function of three independent variables – adsorbent dose (AD,  $X_1$ ), contact time (CT,  $X_2$ ), and initial CV concentration (IC,  $X_3$ ) – a Doehlert matrix combined with RSM was employed. The experimental adsorption capacities of the CV dye by AC- $750^\circ\text{C}$  are given in Table 1.

An analysis of variance was conducted to evaluate the model's validity. As summarized in Table 2, a  $p$ -value below  $0.05$  confirms the statistical significance of the chosen model. Moreover, the high values of the coefficients of determination,  $R^2$ , and adjusted  $R^2$ , illustrate strong agreement between the experimental and theoretical results based on a second-order polynomial equation. Nemrodw software was employed to generate the quadratic polynomial equation corresponding to the adsorption capacity of the CV dye by AC- $750^\circ\text{C}$  (response).

The identification of optimal conditions was derived from a quadratic equation formulated using the Doehlert matrix and selected input variables. Analysis of the experimental data established an empirical relationship between the response

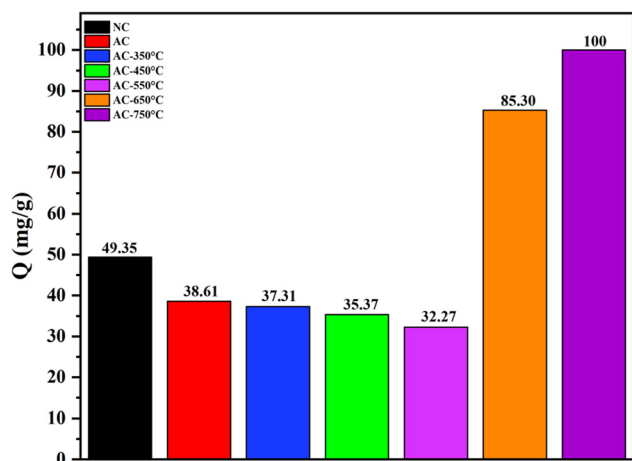


Fig. 4 Adsorption test for CV dye onto NC and MC.

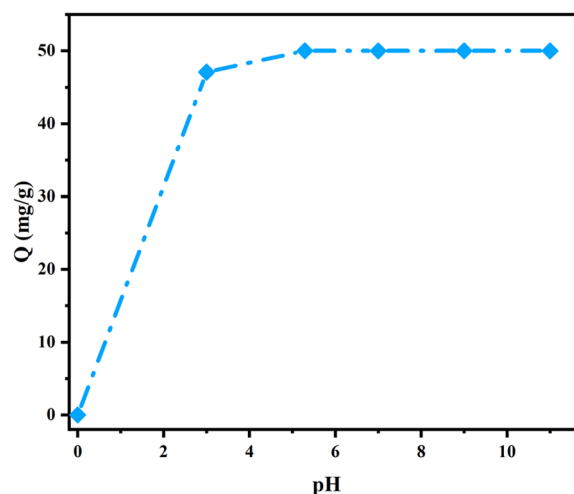


Fig. 5 Variation in the adsorption capacity of CV dye as a function of pH.



**Table 1** Doehlert experimental design and the corresponding determined responses

Runs	$X_1$	$X_2$	$X_3$	AD (g L <sup>-1</sup> )	CT (min)	IC (mg L <sup>-1</sup> )	Adsorption capacity (mg g <sup>-1</sup> ) $Y$
1	1.000	0.000	0.000	2.000	95.000	85.000	42.500
2	-1.000	0.000	0.000	0.400	95.000	85.000	208.880
3	0.500	0.866	0.000	1.600	168.610	85.000	53.120
4	-0.500	-0.866	0.000	0.800	21.380	85.000	84.900
5	0.500	-0.866	0.000	1.600	21.380	85.000	48.270
6	-0.500	0.866	0.000	0.800	168.610	85.000	106.250
7	0.500	0.288	0.816	1.600	119.530	138.070	86.310
8	-0.500	-0.288	-0.816	0.800	70.460	31.920	39.300
9	0.500	-0.288	-0.816	1.600	70.460	31.920	19.920
10	0.000	0.577	-0.816	1.200	144.070	31.920	26.580
11	-0.500	0.288	0.816	0.800	119.530	138.070	172.620
12	0.000	-0.577	0.816	1.200	45.920	138.070	114.990
13	0.000	0.000	0.000	1.200	95.000	85.000	70.830
14	0.000	0.000	0.000	1.200	95.000	85.000	70.830
15	0.000	0.000	0.000	1.200	95.000	85.000	70.830

**Table 2** ANOVA results for the adsorption capacity of CV dye onto AC-750 °C

Factors	Coefficient	Signif. %
Model	—	0.29 <sup>b</sup>
$b_0$	70.83	0.05 <sup>a</sup>
$b_1$	-66.02	0.03 <sup>a</sup>
$b_2$	7.32	39.00
$b_3$	58.81	0.06 <sup>a</sup>
$b_{1-1}$	54.85	1.19 <sup>c</sup>
$b_{2-2}$	-15.20	33.30
$b_{3-3}$	-1.22	93.10
$b_{1-2}$	-9.52	61.90
$b_{1-3}$	-37.61	12.00
$b_{2-3}$	-12.39	56.40
$R^2$	0.969	—
$R^2$ Adj	0.915	—

<sup>a</sup> Statistically significant at the >99.9% level (probability ( $p$ ) < 0.001).

<sup>b</sup> Statistically significant at the >99% level ( $p$ -value < 0.01). <sup>c</sup> Statistically significant at the 95% level ( $p$ -value < 0.05).

( $Y$ ) and the independent factors ( $X_1$ ,  $X_2$ , and  $X_3$ ), as expressed by the following equation (eqn (9)):

$$Y = 70.83 - 66.02X_1 + 7.32X_2 + 58.81X_3 + 54.85X_1^2 - 15.20X_2^2 - 1.22X_3^2 - 9.52X_1X_2 - 37.61X_1X_3 - 12.39X_2X_3 \quad (9)$$

The  $p$ -value was employed for each parameter to assess its significance. The model terms are not significant if the  $p$ -value is above 0.05, but not otherwise ( $p$ -value below 0.05). Terms significant according to the  $p$ -values for ( $X_1$ ,  $X_3$ , and  $X_1^2$ ) were considered significant and retained in the model. After removing the non-significant terms, the final predictive model is presented in eqn (10).

$$Y = 70.83 - 66.02X_1 + 58.81X_3 + 54.85X_1^2 \quad (10)$$

The data obtained were also examined to check the normality of the residuals, as illustrated in Fig. S1a (ESI<sup>†</sup>). According to the plot, the data points are moderately close to a straight line. Furthermore, the graph in Fig. S1b (ESI<sup>†</sup>) shows the residuals as a function of the predicted values, revealing a uniform distribution, with equal dispersion of the residuals below and

above the baseline, signifying that the model maintains a balance in its predictive accuracy. This symmetry also suggests that the mean residual value is close to zero, reinforcing the reliability of the model in predicting the response. As a result, the mathematical model effectively describes the response in relation to experimental conditions.

**3.2.4. Response surface plots.** The influence of different parameters (AD, CT, and IC) and their interaction on the dye removal performance of AC-750 °C was analyzed using eqn (10), 3D response surfaces, as well as 2D contour plots (Fig. 6). The results show that the AD and IC markedly influence the adsorption efficiency. The significant beneficial effect of IC can be explained by the distribution of CV dye molecules through the pores of the AC-750 °C sample, which increases slightly with the dye content, indicating the high affinity between the AC-750 °C surface and the CV dye.<sup>55,56</sup> In contrast, the AD negatively affects the CV dye adsorption capacity. It decreases with increasing AD. This may be explained by the aggregation phenomenon of AC-750 °C particles, which results in a reduction in the adsorbent surface area.<sup>2</sup> The low adsorption efficiency of the CV dye is obtained at the AD between 1.20 and 2.00 g L<sup>-1</sup>. On the other hand, the adsorption capacity of the CV dye was not considerably influenced by CT.

According to the response surfaces and the algebraic regression equations, the optimum operating conditions required to reach the maximum adsorption capacity are shown in Table 3. Adsorption kinetics, isotherms, and thermodynamic studies were performed employing the optimum conditions.

**3.2.5. Kinetics study.** Kinetic models provide essential information on the rate of reaction between the adsorbate and the adsorbent, as well as the factors affecting the rate.<sup>57</sup> The kinetic study of CV adsorption on AC-750 °C was performed using well-known kinetic models, such as PFO, PSO, IPD, and the Elovich model, to identify the most suitable model. The kinetic graphs and parameters of the different models are summarized in Fig. 7 and Table 4. These results indicate that the PSO model effectively describes the adsorption kinetics of CV on AC-750 °C. The value calculated for the maximum adsorption efficiency of the CV dye using AC-750 °C from the linear and non-linear form of PSO is closest to that determined



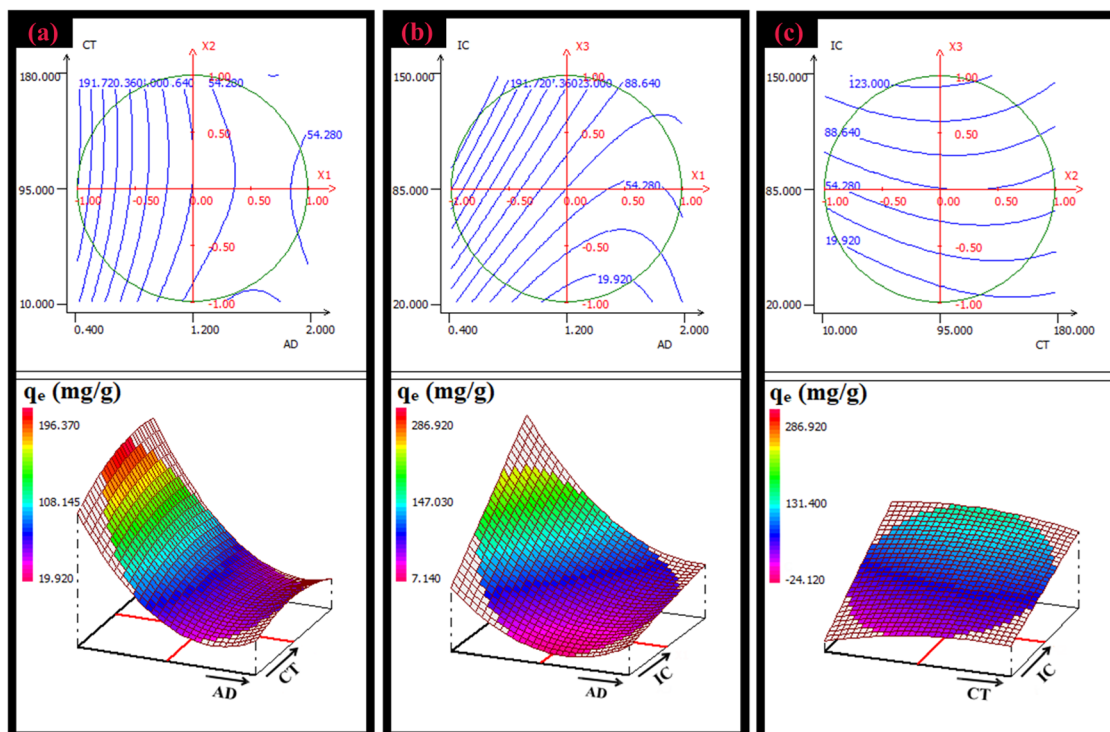


Fig. 6 (a)–(c) 2D–3D surface plots of the variation in the amount of CV dye adsorbed on AC-750 °C as a function of various parameters (AD and CT), (AD and IC), and (CT and IC).

Table 3 Optimum values for the optimal adsorption capacity of CV dye onto AC-750 °C

Parameters	Optimum values	Theoretical adsorption capacity (mg g <sup>-1</sup> )	Experimental adsorption capacity (mg g <sup>-1</sup> )
AD (g L <sup>-1</sup> )	0.50	234.11	236.27
CT (min)	95.00		
IC (mg L <sup>-1</sup> )	118.80		

experimentally. The IPD model was employed to investigate the underlying adsorption mechanism of CV on AC-750 °C.<sup>58</sup> Fig. 7(d) illustrates that the IPD model can be subdivided into three stages. The first linear part indicates the transfer of the adsorbate by boundary layer convection. The second linear part corresponds to diffusion across the boundary layer. Finally, adsorption occurs at the internal adsorption sites, as well as diffusion through the pores and on the outer active sites on the surface of the adsorbent.<sup>58</sup> Moreover, the plots are not linear and do not cross at the origin, confirming not only that the rate of CV dye removal by AC-750 °C is the only rate-determining step, but also that other processes can affect the rate of CV dye removal by AC-750 °C.<sup>56</sup> To determine whether the adsorption process on the heterogeneous surface is chemisorption, the Elovich model was employed.<sup>58</sup> According to the data (Table 4), the adsorption system is a chemical process, specifically an ion exchange process.<sup>59</sup>

Additionally, the equilibrium adsorption capacity value calculated from the non-linear kinetic study showed that the PSF model could also be used to adjust the experimental data. In contrast, the coefficient of determination  $R_m^2$  (Table 4)

calculated using eqn (11) for the PSF model has a value below that of the PSO and Elovich models, indicating that the calculated data correlate well with the PSO and Elovich models. Moreover, the non-linear PSO model exhibits a coefficient of determination  $R_m^2$  close to unity, confirming the chemical reaction involved in dye adsorption.<sup>60</sup>

$$R_m^2 = 1 - \frac{\sum (Q_{e,\text{exp}} - Q_{e,\text{cal}})}{\sum (Q_{e,\text{exp}} - Q_{e,\text{mean}})} \quad (11)$$

**3.2.6. Adsorption isotherms.** Isotherm models were designed to describe the equilibrium adsorption capacities at varying initial concentrations of CV. As depicted in Fig. 8 and Table 5, the Langmuir isotherm model, in both nonlinear and linear forms, proved much more accurate with the experimental data compared to the Freundlich and Temkin models. This result suggests the formation of a monolayer of CV dye on the AC-750 °C surface, where all active adsorption sites possess equivalent adsorption energy, and no interactions occur between the adsorbed molecules.<sup>61</sup> In addition, the maximum





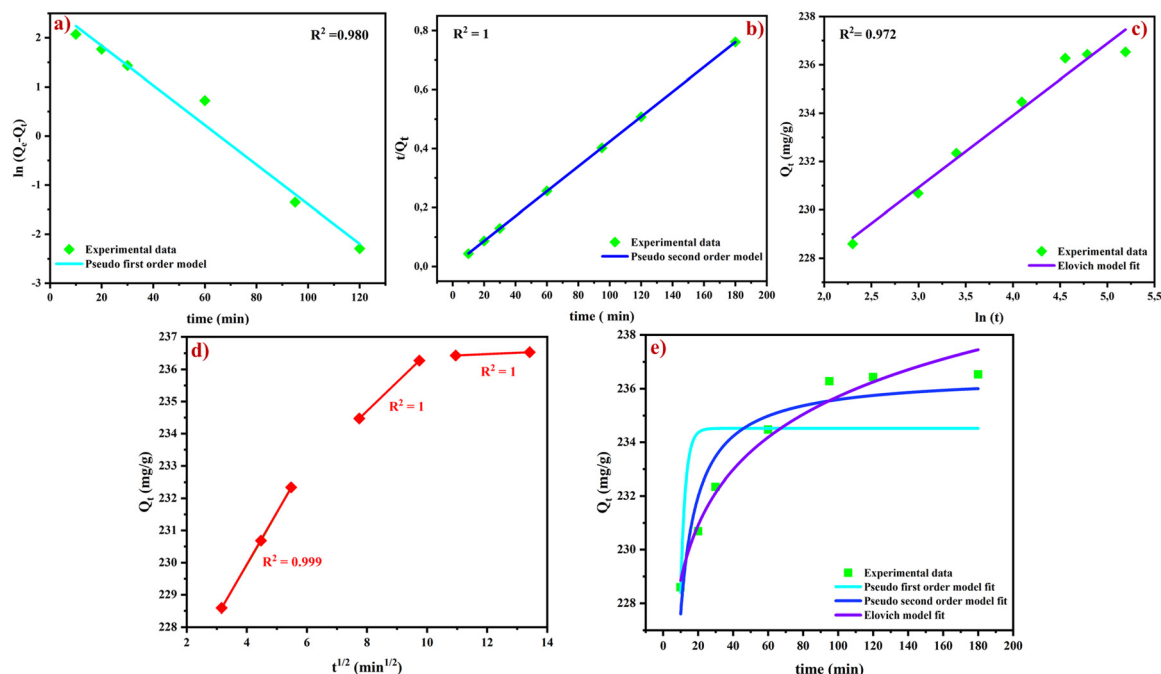


Fig. 7 Linear regression of PSF (a), PSO (b), Elovich (c), and IPD (d) models and (e) nonlinear regression models for CV dye adsorption on AC-750 °C.

Table 4 Kinetic model parameters for CV dye adsorption on AC-750 °C

Kinetic model	Parameters	Non-linear	Linear
PFO	$Q_1$ (mg g <sup>-1</sup> )	234.51	14.08
	$K_1$ (min <sup>-1</sup> )	0.364	0.040
	$R^2$	0.512	0.996
	$R_m^2$	0.51	0.31
PSO	$Q_2$ (mg g <sup>-1</sup> )	236.51	237.52
	$K_2$ (mg g <sup>-1</sup> min <sup>-1</sup> )	0.010	0.007
	$R^2$	0.908	1.000
	$R_m^2$	0.90	0.63
Elovich	$\alpha$ (mg g <sup>-1</sup> min <sup>-1</sup> )	0.282	0.335
	$\beta$ (g mg <sup>-1</sup> )	3.363	3.025
	$R^2$	0.937	0.972
	$R_m^2$	0.73	0.11
IPD	1st stage	$C_1$ (mg g <sup>-1</sup> )	223.47
		$K_{P1}$ (mg g <sup>-1</sup> min <sup>-1/2</sup> )	1.617
		$R^2$	0.999
	2nd stage	$C_2$ (mg g <sup>-1</sup> )	227.50
		$K_{P2}$ (mg g <sup>-1</sup> min <sup>-1/2</sup> )	0.900
		$R^2$	1.000
	3rd stage	$C_3$ (mg g <sup>-1</sup> )	235.98
		$K_{P3}$ (mg g <sup>-1</sup> min <sup>-1/2</sup> )	0.040
		$R^2$	1.000

adsorption capacity ( $Q_{\max}$ ) of the CV dye calculated by the Langmuir model closely matched the experimental value. Moreover, the validity of the Langmuir model can also be confirmed through the equilibrium parameter ( $R_L$ ) (eqn (12)).<sup>62</sup>

$$R_L = \frac{1}{1 + K_L C_0} \quad (12)$$

Here,  $C_0$  (mg L<sup>-1</sup>) and  $K_L$  (L mg<sup>-1</sup>) are the initial CV dye concentration and the Langmuir constant, respectively. Indeed,

if  $0 < R_L < 1$ , the adsorption process can be considered favorable and irreversible if  $R_L = 0$ , and linear for  $R_L = 1$  or unfavorable if  $R_L > 1$ .<sup>63</sup> The  $R_L$  value calculated in this study is in the 0–1 range, confirming that CV dye adsorption is more favorable on AC-750 °C.

To evaluate how well the isotherm equations fit the experimental data, the coefficient of determination ( $R_m^2$ ) was calculated and displayed in Table 5. The results show that the non-linear Langmuir isotherm model fits the experimental equilibrium adsorption data well, based on the highest coefficient of determination values, indicating a monolayer process.

Table 6 compares the performance of the adsorbent synthesized in this work with that of other adsorbents, such as activated carbon and composites, for the adsorption of CV dye. According to the data, AC-750 °C has a higher adsorption capacity than other adsorbents. Moreover, it is notable that in most previous studies, the maximum adsorption capacity was achieved under alkaline pH conditions. In a few studies, high adsorption capacity was achieved at a pH below 7, but the capacity was much lower compared to that of AC-750 °C.

**3.2.7. Thermodynamic study.** This study focuses on evaluating the values of different variables, including Gibbs free energy ( $\Delta G$ ), enthalpy ( $\Delta H$ ), and entropy ( $\Delta S$ ), to examine the effect of temperature on the efficiency of CV dye removal by AC-750 °C. The value of each parameter was calculated using the following equations.<sup>68,69</sup>

$$K_d = \frac{q_e}{C_e} \quad (13)$$

$$\Delta G = -RT \ln K_d \quad (14)$$



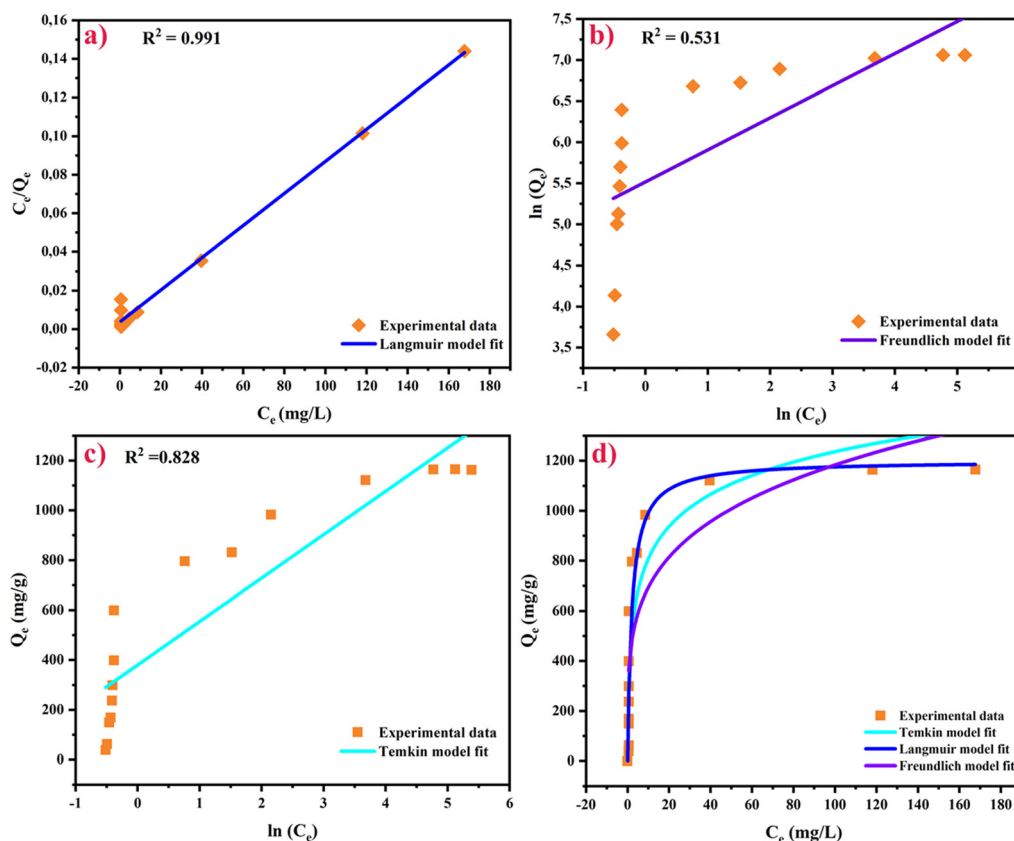


Fig. 8 Linear regression of the Langmuir (a), Freundlich (b), and Temkin models (c), and (d) non-linear isotherms for CV dye adsorption on AC-750 °C.

Table 5 The main parameters of the different isotherm models

Isotherms	Parameters	Non-linear	Linear
Langmuir	$Q_m$ (mg g <sup>-1</sup> )	1199.93	1201.58
	$K_L$ (L mg <sup>-1</sup> )	0.47	0.228
	$R_L$	0.096	0.179
	$R^2$	0.900	0.991
	$R_m^2$	0.90	0.56
Freundlich	$n$	4.30	2.55
	$K_F$ (mg <sup>(1-n)</sup> L <sup>n</sup> g <sup>-1</sup> )	405.98	248.58
	$R^2$	0.718	0.531
	$R_m^2$	0.69	0.12
Temkin	$B$ (J mol <sup>-1</sup> )	186.26	174.20
	$K_T$ (L mg <sup>-1</sup> )	7.62	8.58
	$R^2$	0.839	0.828
	$R_m^2$	0.80	0.80

$$\Delta G = \Delta H - T\Delta S \quad (15)$$

$$\ln K_d = \frac{\Delta S}{R} - \frac{\Delta H}{RT} \quad (16)$$

$K_d$ ,  $q_e$  (mg g<sup>-1</sup>),  $C_e$  (mg L<sup>-1</sup>),  $T$ , and  $R$  are the distribution coefficient, equilibrium adsorption capacity, equilibrium concentration, temperature, and the ideal gas constant, respectively.

Fig. 9 illustrates the effect of temperature on the  $\ln K_d$  value. A straight line is given by plotting  $\ln K_d$  against  $1/T$ . This allows us to determine the parameters ( $\Delta H$  and  $\Delta S$ ) as a function of

the slope and the intercept, respectively. The values of  $\Delta G$  can be calculated using eqn (15). The values of the various thermodynamic parameters at different temperatures are given in Table 7.

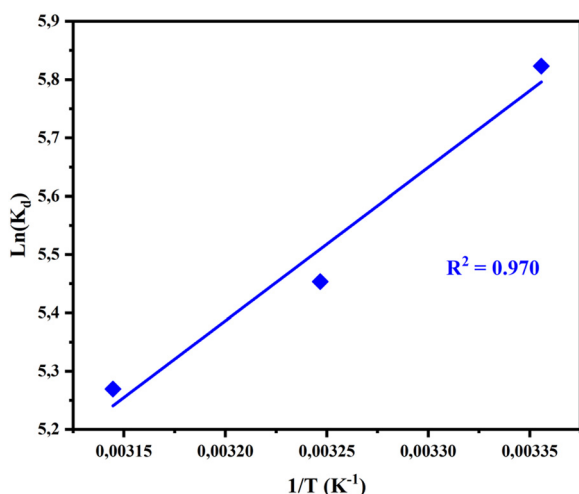
The adsorption of the CV dye on AC-750 °C, over the temperature range, shows negative values of  $\Delta G$ , confirming the spontaneity of the adsorption process.<sup>70</sup> In addition, the negative value of  $\Delta G$  decreases with increasing temperature, indicating that the adsorption process becomes highly favorable at lower temperatures.<sup>71</sup> The negative value of  $\Delta H$  confirms the exothermic behavior of CV dye removal by AC-750 °C.<sup>72,73</sup> In the meantime, the negative value of  $\Delta S$  implied a decrease in randomness at the adsorbent/adsorbate interface.<sup>72</sup>

**3.2.8. Reusability study of AC-750 °C.** The process of regenerating spent adsorbent is crucial for the practical removal of pollutants in industrial applications to ensure the use of the adsorbent in repetitive cycles and thus minimize costs. To this end, various desorption agents, including 0.1 M KOH, 0.1 M HCl, thermal treatment at 350, 550, and 650 °C, ethanol, and ethanol/thermal treatment at 750 °C, were investigated for regenerating AC-750 °C@CV (Table 8). The results demonstrate an improvement in desorption efficiency with increasing temperatures, but it remains lower. In addition, the ethanol solvent alone shows a lower efficiency in removing the CV dye during the desorption process compared to the combined ethanol solvent and thermal treatment at 750 °C, which gave the best



**Table 6** Comparison of the maximum adsorption capacity of CV obtained with AC-750 °C in this study and other adsorbents

Adsorbents	Optimum conditions	Adsorption capacity (mg g <sup>-1</sup> )	Adsorption isotherms	Reference
AC-750 °C	<ul style="list-style-type: none"> <li>AD = 0.5 g L<sup>-1</sup></li> <li>pH = 5.29</li> <li>IC = 750 mg L<sup>-1</sup></li> </ul>	1199.93	Langmuir	This work
Heat-Treated Brazilian Palygorskite	<ul style="list-style-type: none"> <li>AD = 2 g L<sup>-1</sup></li> <li>pH = 7</li> <li>IC = 200 mg L<sup>-1</sup></li> </ul>	186.5	Langmuir	64
Muscovite clay	<ul style="list-style-type: none"> <li>AD = 1.5 g L<sup>-1</sup></li> <li>pH = 6</li> <li>IC = 70 mg L<sup>-1</sup></li> </ul>	69.54	Langmuir	37
Activated carbon	<ul style="list-style-type: none"> <li>AD = 1 g L<sup>-1</sup></li> <li>pH = 8.5</li> <li>IC = 750 mg L<sup>-1</sup></li> </ul>	496.55	Langmuir	65
Polypyrrole-decorated bentonite magnetic nanocomposite	<ul style="list-style-type: none"> <li>AD = 2 g L<sup>-1</sup></li> <li>pH = 8</li> <li>IC = 100 mg L<sup>-1</sup></li> </ul>	98.04	Langmuir	66
Composite (Ch-IL@SPEEK)	<ul style="list-style-type: none"> <li>AD = 1 g L<sup>-1</sup></li> <li>pH = 5.21–5.35</li> <li>IC = 50 mg L<sup>-1</sup></li> </ul>	77.66	Langmuir	67

**Fig. 9** Van't Hoff plot for CV dye adsorption onto AC-750 °C.**Table 7** Principal thermodynamic parameters for CV dye adsorption on AC-750 °C

T (K)	ln (K <sub>d</sub> )	ΔG (kJ mol <sup>-1</sup> )	ΔH (kJ mol <sup>-1</sup> )	ΔS (J K <sup>-1</sup> mol <sup>-1</sup> )
298	5.82	−14.35	−21.87	−25.23
308	5.45	−14.09		
318	5.26	−13.84		

results in the desorption test (Table 8). The ethanol solvent lacks the energy required to break the bonds formed during the adsorption process, known as chemisorption. Dissolved organic carbon could be removed by thermal treatment. Subsequently, combining ethanol solvent and thermal treatment at 750 °C can effectively break the bonds between the CV dye and AC-750 °C, regenerating the AC-750 °C adsorbent for

subsequent adsorption cycles. Similarly, a study of MB desorption by Mohammad *et al.*<sup>74</sup> demonstrated that using various solvents such as ethanol, hydrochloric acid, nitric acid, or acetone, and heating alone did not provide sufficient energy to break the bonds between the adsorbate and the adsorbent. Furthermore, the same study highlighted the effect of temperature on dye desorption efficiency, revealing an enhancement in desorption efficiency with temperature owing to the improvement in adsorbate solubility and the distribution coefficient as a function of temperature.<sup>74</sup> Consequently, a chemical and thermal treatment at higher temperatures was necessary to regenerate the adsorbent effectively. Fig. 10(a) illustrates the regeneration capacity of AC-750 °C over three adsorption-desorption cycles. A continuous decrease in removal efficiency was observed after each reuse; however, three cycles of AC-750 °C were the most effective and still retained 50% efficiency. This decrease can be attributed to the cumulative effects of several treatment processes. However, these results revealed the reliability and durability of AC-750 °C for use in multiple applications to remove the CV dye from aqueous solutions.

The AC-750 °C regenerated adsorbent was characterized using XRD and SEM analyses. As illustrated in Fig. 10(b), the peaks assigned to muscovite, positioned at  $2\theta = 40.25$  and  $42.41^\circ$ , were not significantly altered. In contrast, the diffraction peaks at  $2\theta = 8.78^\circ$ ,  $18.02^\circ$ ,  $19.82^\circ$ ,  $27.50^\circ$ ,  $27.96^\circ$ , and  $34.14^\circ$ , attributed to muscovite, were drastically reduced after the regeneration process. These results confirm the change in adsorption capacity of the AC-750 °C material. The spectra of AC-750 °C and the AC-750 °C were almost identical, despite the reported variation in the intensity of some peaks, indicating the structural stability of AC-750 °C. For SEM images (Fig. 10(c)), the results reveal an increase in grain size after subsequent heat treatments, making the surface of AC-750 °C denser, and thus limiting the active site for the adsorption process. In addition,



Table 8 Regeneration study using multiple agents

	Ethanol/thermal treatment (750 °C)	Ethanol	0.1 M (HCl)	0.1 M (KOH)	350 °C	550 °C	650 °C
First reuse	86.50%	11.14%	1.34%	3.58%	1.14%	5.20%	7.32%
Second reuse	60.27%	—	—	—	—	—	—
Third reuse	57.82%	—	—	—	—	—	—

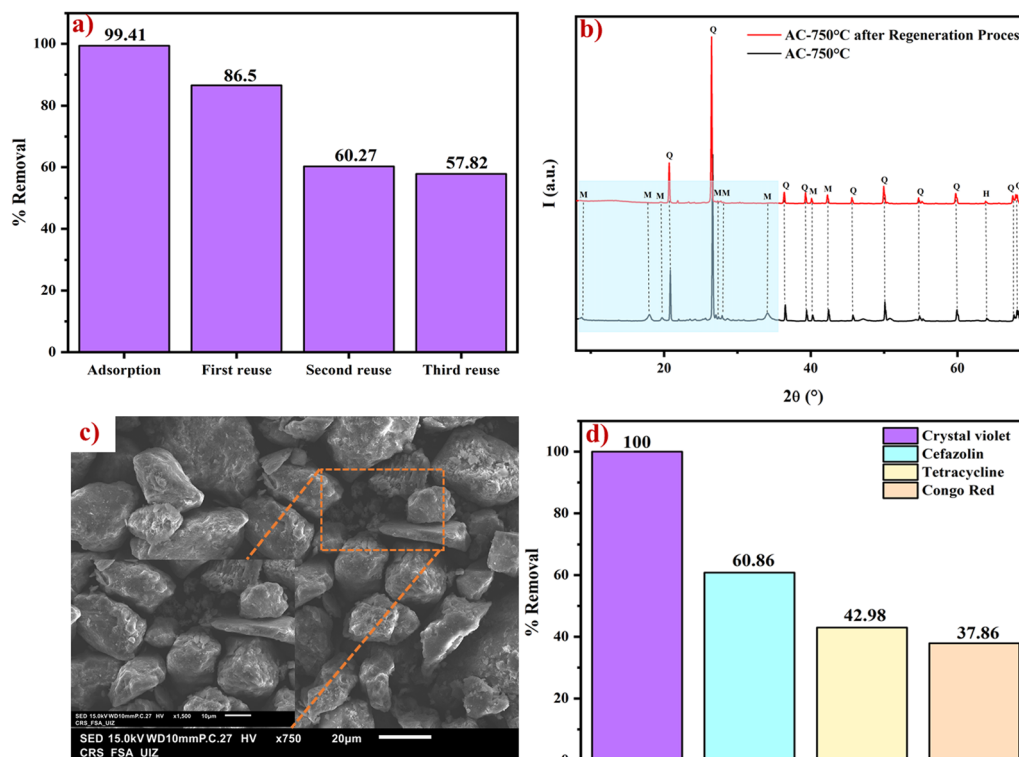


Fig. 10 Recyclability experiment (a) of AC-750 °C for CV dye removal, XRD pattern (b) for AC-750 °C before and after the regeneration process, SEM images (c) of AC-750 °C after the regeneration process, and percentage removal (d) of various organic pollutants using AC-750 °C.

SEM characterization revealed that AC-750 °C retained a stable structure after several cycles, underlining its potential for effective reuse in adsorption applications.

### 3.2.9. Selectivity of AC-750 °C towards organic pollutants.

Fig. 10(c) shows the capacity of AC-750 °C towards four organic pollutants: dyes (CV and Congo red) and antibiotics (cefazoline and tetracycline). The experiments were carried out under the same AD ( $1 \text{ g L}^{-1}$ ) and IC ( $50 \text{ mg L}^{-1}$ ) at the natural pH of each pollutant. The results revealed that the maximum percentage removal was achieved for the CV dye. Furthermore, the AC-750 °C adsorbent exhibits a high and moderate percentage removal of cefazolin and tetracycline, respectively. On the other hand, the percentage of Congo red removal remained lower. Therefore, AC-750 °C could be selected as a better adsorbent for removing antibiotics and cationic dyes.

**3.2.10. Adsorption mechanism analysis.** The mechanism of CV dye removal by AC-750 °C was analyzed using FTIR, SEM-EDS, and the  $\text{pH}_{\text{pzc}}$ . Fig. 11(a) shows the FTIR spectrum of AC-750 °C before and after the CV dye removal. The results show that the main bands of the AC-750 °C material exhibit several changes after adsorption of CV dye molecules,

indicating that various mechanisms may govern CV adsorption. The electrostatic interactions between the permanent negative charge of Si–O–Si groups of AC-750 °C and the positive charge of the nitrogen atoms in the CV dye constitute the key mechanism of the adsorption process.<sup>75</sup> This can be clearly illustrated by the decrease in intensity of the Si–O–Si band. The decrease in intensity of –OH and the shifting of the Al–Al–OH band confirm the involvement of hydrogen bonding between OH groups and nitrogen atoms of CV dye molecules.<sup>72</sup> In addition, a significant change in the Si–O bond intensity may lead to a hydrogen bond between the oxygen atoms of Si–O groups and the hydrogen atoms of –CH<sub>3</sub> groups belonging to the CV dye structure.<sup>76</sup> These findings are confirmed by the formation of new peaks at 1373 and 1173  $\text{cm}^{-1}$  attributed to C–H bonds of the aromatic ring.<sup>72,76,77</sup> Furthermore, a possible mechanism involves the n– $\pi$  interaction between the non-bonding doublet of oxygen atoms of Si–O groups and the C=C bonds of the CV dye molecules.<sup>72,78</sup> A peak at 1325  $\text{cm}^{-1}$  is linked to C–N bonds in the dye structure.<sup>79</sup> Other peaks also appeared at 1238 and 1287  $\text{cm}^{-1}$ , confirming the adsorption process. Finally, a cation exchange mechanism might occur due to the substitution of





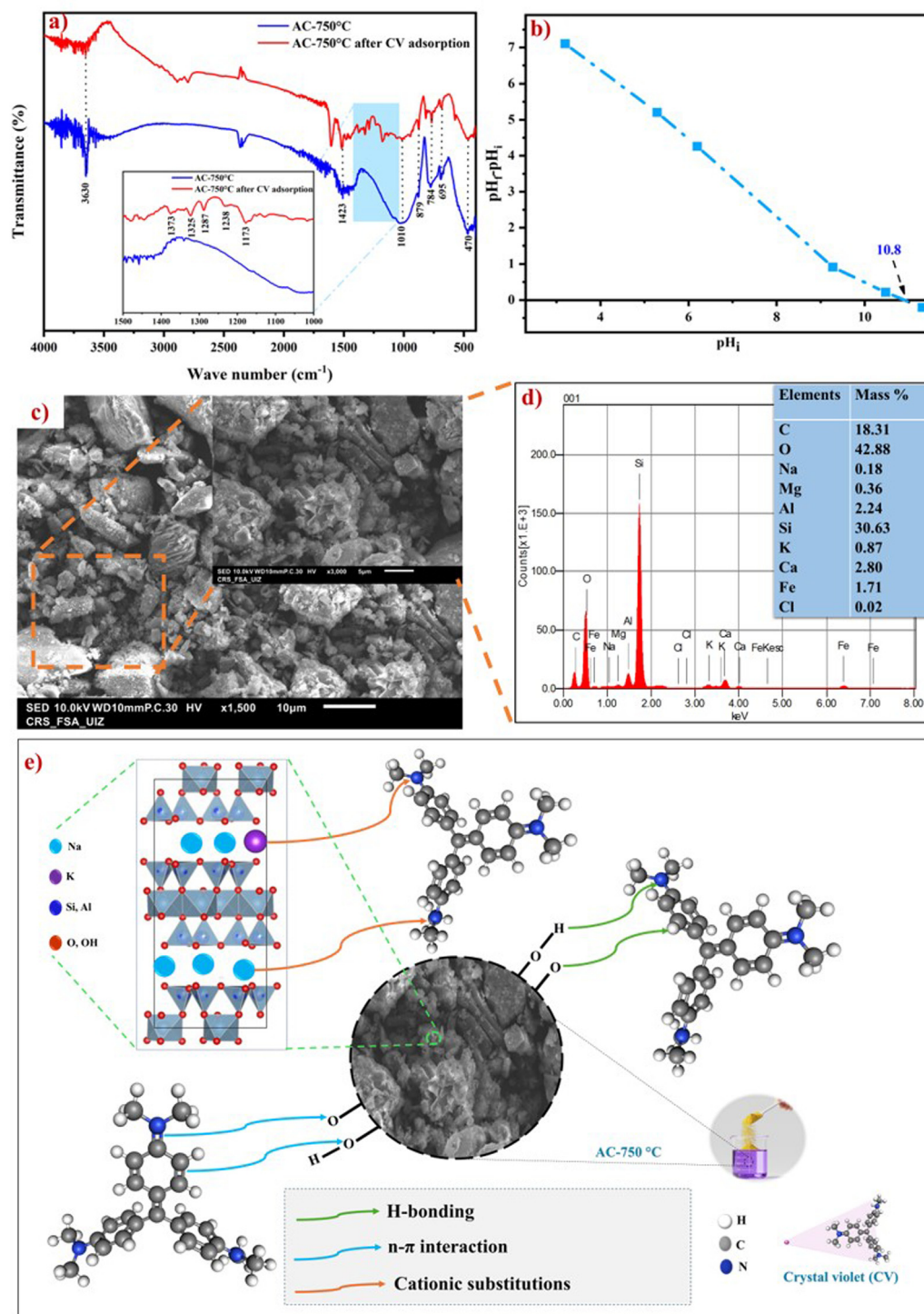


**Fig. 11** FTIR spectra of (a) AC-750 °C and AC-750 °C@CV, pH<sub>pzc</sub> of (b) AC-750 °C, SEM images (c) and EDS analysis (d) of AC-750 °C@CV, and graphical illustration (e) of CV dye removal using AC-750 °C.

potassium or sodium cations by the organic cations of the CV dye.<sup>19,37</sup>

Determining the zero-charge point (pH<sub>pzc</sub>) is crucial for understanding the mechanism of adsorption. This determination was carried out by plotting the change in pH (pH<sub>final</sub> – pH<sub>initial</sub>) as a function of the initial pH of the solution, as shown

in Fig. 11(b). The results indicate that the pH<sub>pzc</sub> value for AC-750 °C is approximately 10.8. These results reveal that the surface of AC-750 °C is positively charged at pH < pH<sub>pzc</sub> and negatively charged at pH > pH<sub>pzc</sub>, respectively, confirming that there is no electrostatic interaction between the CV dyes and AC-750 °C after the adsorption of CV dyes at pH = 5.29.

Fig. 11(c) shows the SEM images of AC-750 °C after the adsorption process. The morphology of AC-750 °C became more heterogeneous than that of AC-750 °C, confirming the successful CV dye adsorption on AC-750 °C. EDS analysis (Fig. 11(d)) indicated an increase in carbon (C) content and the appearance of chlorine (Cl) after CV dye adsorption, suggesting the presence of CV dye on the AC-750 °C surface. Based on the mentioned analysis, a possible adsorption mechanism is illustrated in Fig. 11(e).

## 4. Conclusion

The outcome of this study demonstrates the effectiveness of combining basic activation and thermal treatment on the adsorption capacity of CV dye. The AC-750 °C was chosen as the most promising adsorbent for the removal of CV dye. It demonstrated a higher adsorption capacity of 1199.93 mg g<sup>-1</sup>, and a high value of dye removal of 99.41% under the following conditions: an AD of 0.5 g L<sup>-1</sup>, a CT of 95 min, and IC of 750 mg L<sup>-1</sup> at a natural pH of 5.29. The PSO nonlinear model was well suited to the kinetic study. Furthermore, equilibrium data revealed that the non-linear Langmuir model was the appropriate model to characterize the removal process of CV molecules on AC-750 °C. Finally, the thermodynamic study showed that the adsorption of CV dye onto AC-750 °C was spontaneous and exothermic. Based on the findings, the natural clay activated with Na<sub>2</sub>CO<sub>3</sub> and calcined at 750 °C can be considered an environmentally friendly and effective adsorbent for removing the CV dye. At the same time, the modification process that combines basic activation with thermal treatment is an economical method for enhancing the properties of clays, especially their adsorption properties.

## Data availability

All required data are summarized in this manuscript and the ESI.†

## Conflicts of interest

The authors declare that they have no known competing financial interests or personal relationships that could have appeared to influence the work reported in this paper.

## Acknowledgements

We extend our heartfelt gratitude to the Moroccan Ministry of Higher Education, Scientific Research and Innovation, for funding this work as part of the PhD Associate Scholarship (PASS). We would also like to thank Ibn Zohr University for the invaluable administrative and technical assistance.

## References

- 1 P. Yang, Y. Lu, H. Zhang, R. Li, X. Hu, A. Shahab, A. Y. Elnaggar, A. F. Alrefaei, M. H. Almutairi and E. Ali, Effective removal of methylene blue and crystal violet by low-cost biomass derived from eucalyptus: Characterization, experiments, and mechanism investigation, *Environ. Technol. Innovation*, 2024, **33**, 103459.
- 2 M. Boulahbal, M. A. Malouki, M. Canle, Z. Redouane-Salah, S. Devanesan, M. S. AlSalhi and M. Berkani, Removal of the industrial azo dye crystal violet using a natural clay: Characterization, kinetic modeling, and RSM optimization, *Chemosphere*, 2022, **306**, 135516.
- 3 Y. El Ouardi, V. Lenoble, C. Branger, K. Laatikainen, B. Angeletti and A. Ouammou, Enhancing clay adsorption properties: a comparison between chemical and combined chemical/thermal treatments, *Groundw. Sustain. Dev.*, 2021, **12**, 100544.
- 4 L. Velarde, M. S. Nabavi, E. Escalera, M.-L. Antti and F. Akhtar, Adsorption of heavy metals on natural zeolites: A review, *Chemosphere*, 2023, **328**, 138508.
- 5 H. Ouaddari, B. Abbou, I. Lebkiri, A. Habsaoui, M. Ouzzine and R. F. Allah, Removal of Methylene Blue by adsorption onto natural and purified clays: Kinetic and thermodynamic study, *Chem. Phys. Impact*, 2024, **8**, 100405.
- 6 R. Dhanabal and P. G. Priya, Optimization and photocatalytic degradation of crystal violet dye using Sr-ZnO/activated carbon nanoneedles, *Mater. Sci. Semicond. Process.*, 2025, **192**, 109481.
- 7 A. A. Oyekanmi, K. K. Katibi, R. C. Omar, A. Ahmad, M. Elbidi, M. B. Alshammari and I. G. Shitu, A novel oil palm frond magnetic biochar for the efficient adsorption of crystal violet and sunset yellow dyes from aqueous solution: synthesis, kinetics, isotherm, mechanism and reusability studies, *Appl. Water Sci.*, 2024, **14**, 13.
- 8 A. O. Adeleke, R. C. Omar, K. K. Katibi, T. T. Dele-Afolabi, A. Ahmad, J. O. Quazim, A. A. Amusa and M. B. Alshammari, Process optimization of superior biosorption capacity of biogenic oyster shells nanoparticles for Congo red and Bromothymol blue dyes removal from aqueous solution: Response surface methodology, equilibrium isotherm, kinetic, and reusability studies, *Alexandria Eng. J.*, 2024, **92**, 11–23.
- 9 M. A. Rosli, Z. Daud, H. Awang, A. A. A. Latiff, A. Zainorabidin and A. A. Halim, The effectiveness of peat-AC composite adsorbent in removing SS, colour and Fe from landfill leachate, *Int. J. Integr. Eng.*, 2017, **9**, 35–38.
- 10 S. Mustapha, M. M. Ndamitso, A. S. Abdulkareem, J. O. Tijani, A. K. Mohammed and D. T. Shuaib, Potential of using kaolin as a natural adsorbent for the removal of pollutants from tannery wastewater, *Heliyon*, 2019, **5**, e02923.
- 11 T. Ngulube, J. R. Gumbo, V. Masindi and A. Maity, An update on synthetic dyes adsorption onto clay based minerals: A state-of-art review, *J. Environ. Manage.*, 2017, **191**, 35–57.



- 12 A. Kausar, M. Iqbal, A. Javed, K. Aftab, H. N. Bhatti and S. Nouren, Dyes adsorption using clay and modified clay: A review, *J. Mol. Liq.*, 2018, **256**, 395–407.
- 13 E. Hussain, A. Ahtesham, M. Shahadat, M. N. M. Ibrahim and S. Ismail, Recent advances of Clay/polymer-based nano-materials for the treatment of environmental contaminants in wastewater: A review, *J. Environ. Chem. Eng.*, 2024, **11**, 112401.
- 14 K. Samrane and A. Bouhaouss, Experimental tests of cadmium and trace metals adsorption on natural clays and activated carbon from wet phosphoric acid, *Inorg. Chem. Commun.*, 2022, **144**, 109866.
- 15 B. Messaid, I. Djemai, I. Boudouh and M. D. Robustillo, Assessment of the performance of an acid-activated composite made of Na-montmorillonite Algerian clay to remove phenol and 4-chlorophenol from water, *Desalin. Water Treat.*, 2025, **322**, 101088.
- 16 D. Ewis, M. M. Ba-Abbad, A. Benamor and M. H. El-Naas, Adsorption of organic water pollutants by clays and clay minerals composites: A comprehensive review, *Appl. Clay Sci.*, 2022, **229**, 106686.
- 17 J. O. Eniola, R. Kumar, M. A. Barakat and J. Rashid, A review on conventional and advanced hybrid technologies for pharmaceutical wastewater treatment, *J. Cleaner Prod.*, 2022, **356**, 131826.
- 18 K. Bahranowski, A. Klimek, A. Gaweł and E. M. Serwicka, Rehydration driven Na-activation of bentonite—Evolution of the clay structure and composition, *Materials*, 2021, **14**, 7622.
- 19 E. Padilla-Ortega, N. Medellín-Castillo and A. Robledo-Cabrera, Comparative study of the effect of structural arrangement of clays in the thermal activation: Evaluation of their adsorption capacity to remove Cd(II), *J. Environ. Chem. Eng.*, 2020, **8**, 103850.
- 20 J. O. Eniola, B. Sizirici, S. Stephen, I. Yildiz, A. Khaleel and M. El Fadel, A new synthesis route of hydrothermally carbonized Na<sub>2</sub>CO<sub>3</sub> activated bentonite-clay as a novel adsorbent for cadmium removal from wastewater, *Sep. Purif. Technol.*, 2024, **350**, 127960.
- 21 S. Barakan and V. Aghazadeh, The advantages of clay mineral modification methods for enhancing adsorption efficiency in wastewater treatment: a review, *Environ. Sci. Pollut. Res.*, 2021, **28**, 2572–2599.
- 22 S. Hamdi, H. Gharbi-Khelifi, A. Barreiro, M. Mosbahi, R. Cela-Dablanca, J. Brahmi, M. J. Fernández-Sanjurjo, A. Núñez-Delgado, M. Issaoui and E. Álvarez-Rodríguez, Tetracycline adsorption/desorption by raw and activated Tunisian clays, *Environ. Res.*, 2024, **242**, 117536.
- 23 A. Imgharn, L. Anchoum, A. Hsini, Y. Naciri, M. Laabd, M. Mobarak, N. Aarab, A. Bouziani, S. Szunerits and R. Boukherroub, Effectiveness of a novel polyaniline@Fe-ZSM-5 hybrid composite for Orange G dye removal from aqueous media: Experimental study and advanced statistical physics insights, *Chemosphere*, 2022, **295**, 133786.
- 24 Z. Mchich, B. Kjidaa, T. Bouzid, N. Saffaj, M. El Haddad and R. Mamouni, Engineering of highly bio-adsorbent Zinc Oxide/Cellana Tramoserica seashells for efficient removal of anionic dye: BBD optimization, density functional theory study, and adsorption mechanism, *Sep. Purif. Technol.*, 2025, **132015**.
- 25 E. Ben Khalifa, B. Rzig, R. Chakroun, H. Nouagui and B. Hamrouni, Application of response surface methodology for chromium removal by adsorption on low-cost biosorbent, *Chemom. Intell. Lab. Syst.*, 2019, **189**, 18–26.
- 26 E. Ben Khalifa, C. Cecone, B. Rzig, S. Azaiez, F. Cesano, M. Malandrino, P. Bracco and G. Magnacca, Green surface modification of polyvinyl alcohol fibers and its application for dye removal using Doehlert experimental design, *React. Funct. Polym.*, 2023, **193**, 105763.
- 27 D. Mathieu, J. Nony and R. Phan-Tan-Luu, *Nemrod-W Software*, LPRAI, Marseille, 2000.
- 28 D. Mathieu, J. Nony and R. Phan-Tan-Luu, *LPRAI, Logiciel Nemrod*, LPRAI, Marseille, 2009.
- 29 N. Dobe, D. Abia, C. Tcheka, J. P. N. Tejeogue and M. Harouna, Removal of amaranth dye by modified Ngassa clay: Linear and non-linear equilibrium, kinetics and statistical study, *Chem. Phys. Lett.*, 2022, **801**, 139707.
- 30 A. Q. Selim, E. A. Mohamed, M. K. Seliem and A. M. Zayed, Synthesis of sole cancrinite phase from raw muscovite: Characterization and optimization, *J. Alloys Compd.*, 2018, **762**, 653–667.
- 31 F. Gridi-Bennadji, B. Beneu, J.-P. Laval and P. Blanchart, Structural transformations of muscovite at high temperature by X-ray and neutron diffraction, *Appl. Clay Sci.*, 2008, **38**, 259–267.
- 32 J. Mañosa, A. Alvarez-Coscojuela, J. Marco-Gibert, A. Maldonado-Alameda and J. M. Chimenos, Enhancing reactivity in muscovitic clays: Mechanical activation as a sustainable alternative to thermal activation for cement production, *Appl. Clay Sci.*, 2024, **250**, 107266.
- 33 E. Mariani, K. H. Brodie and E. H. Rutter, Experimental deformation of muscovite shear zones at high temperatures under hydrothermal conditions and the strength of phyllosilicate-bearing faults in nature, *J. Struct. Geol.*, 2006, **28**, 1569–1587.
- 34 S. Guggenheim, Y.-H. Chang and A. F. Koster, van Groos, Muscovite dehydroxylation; high-temperature studies, *Am. Mineral.*, 1987, **72**, 537–550.
- 35 M. El-Habacha, S. Lagdali, A. Dabagh, G. Mahmoudy, A. Assouani, M. Benjelloun, Y. Miyah, S. Iaich, M. Chiban and M. Zerbet, High efficiency of treated-phengite clay by sodium hydroxide for the Congo red dye adsorption: optimization, cost estimation, and mechanism study, *Environ. Res.*, 2024, **259**, 119542.
- 36 O. Amrhar, A. Berisha, L. El Gana, H. Nassali and M. S. Elyoubi, Removal of methylene blue dye by adsorption onto Natural Muscovite Clay: experimental, theoretical and computational investigation, *Int. J. Environ. Anal. Chem.*, 2023, **103**, 2419–2444.
- 37 S. Ssouni, Y. Miyah, M. Benjelloun, F. Mejbar, M. El-Habacha, S. Iaich, A. A. Addi and A. Lahrichi, High-performance of muscovite clay for toxic dyes' removal:





- Adsorption mechanism, response surface approach, regeneration, and phytotoxicity assessment, *Case Stud. Chem. Environ. Eng.*, 2023, **8**, 100456.
- 38 B. Öztop and T. Shahwan, Modification of a montmorillonite-illite clay using alkaline hydrothermal treatment and its application for the removal of aqueous  $\text{Cs}^+$  ions, *J. Colloid Interface Sci.*, 2006, **295**, 303–309.
  - 39 A. Aboussabek, L. Boukarma, S. El Qdhy, A. Ousaa, M. Zerbet and M. Chiban, Experimental investigation, kinetics and statistical modeling of methylene blue removal onto  $\text{Clay@Fe}_3\text{O}_4$ : Batch, fixed bed column adsorption and photo-Fenton degradation studies, *Case Stud. Chem. Environ. Eng.*, 2024, **9**, 100580.
  - 40 S. Tetteh, A. Quashie and M. A. Anang, Purification, Characterization, and Time-Dependent Adsorption Studies of Ghanaian Muscovite Clay, *J. Chem.*, 2018, **2018**, 6252913.
  - 41 S. Hamdi, M. Mosbahi, M. Issaoui, A. Barreiro, R. Cela-Dablanca, J. Brahmi, A. Tlili, F. Jamoussi, M. J. Fernández-Sanjurjo and A. Núñez-Delgado, Experimental data and modeling of sulfadiazine adsorption onto raw and modified clays from Tunisia, *Environ. Res.*, 2024, **248**, 118309.
  - 42 L. Heller-Kallai and I. Lapidés, Dehydroxylation of muscovite: study of quenched samples, *Phys. Chem. Miner.*, 2015, **42**, 835–845.
  - 43 L. Heller-Kallai and L. I. Rozenson, Dehydroxylation of dioctahedral phyllosilicates, *Clays Clay Miner.*, 1980, **28**, 355–368.
  - 44 M. Thommes, K. Kaneko, A. V. Neimark, J. P. Olivier, F. Rodriguez-Reinoso, J. Rouquerol and K. S. W. Sing, Physisorption of gases, with special reference to the evaluation of surface area and pore size distribution (IUPAC Technical Report), *Pure Appl. Chem.*, 2015, **87**, 1051–1069.
  - 45 F. M. Jais, C. Y. Chee, Z. Ismail and S. Ibrahim, Experimental design via NaOH activation process and statistical analysis for activated sugarcane bagasse hydrochar for removal of dye and antibiotic, *J. Environ. Chem. Eng.*, 2021, **9**, 104829.
  - 46 A. M. Badawy, A. A. Farghali, A. Bonilla-Petriciolet, A. Q. Selim and M. K. Seliem, Effective removal of  $\text{Cr}(\text{VI})$  and methyl orange by nano magnetite loaded starch/muscovite biocomposite: Characterization, experiments, advanced modeling, and physicochemical parameters interpretation, *Int. J. Biol. Macromol.*, 2023, **224**, 1052–1064.
  - 47 A. Lachehab, O. Mertah, A. Kherbeche and H. Hassoune, Utilization of phosphogypsum in  $\text{CO}_2$  mineral sequestration by producing potassium sulphate and calcium carbonate, *Mater. Sci. Energy Technol.*, 2020, **3**, 611–625.
  - 48 D. Simón, C. P. Battistessa, D. C. Arduzzo, S. Gass and A. Cristóbal, Valorization of sludge from the effluent treatment of the dairy industry as clay substitutes in building bricks, *Constr. Build. Mater.*, 2021, **307**, 124955.
  - 49 R. Sposito, N. Beuntner and K.-C. Thienel, Characteristics of components in calcined clays and their influence on the efficiency of superplasticizers, *Cem. Concr. Compos.*, 2020, **110**, 103594.
  - 50 F. Jia, J. Su and S. Song, Can natural muscovite be expanded?, *Colloids Surf., A*, 2015, **471**, 19–25.
  - 51 X. Guo, Z. Wu, Z. Wang, F. Lin, P. Li and J. Liu, Preparation of chitosan-modified bentonite and its adsorption performance on tetracycline, *ACS Omega*, 2023, **8**, 19455–19463.
  - 52 S. Aytas, M. Yurtlu and R. Donat, Adsorption characteristic of  $\text{U}(\text{VI})$  ion onto thermally activated bentonite, *J. Hazard. Mater.*, 2009, **172**, 667–674.
  - 53 R. A. S. Alatawi, Electrospun nanofiber chitosan/polyvinyl alcohol loaded with metal organic framework nanofiber for efficient adsorption and removal of industrial dyes from waste water: Adsorption isotherm, kinetic, thermodynamic, and optimization via Box-Behnken design, *Int. J. Biol. Macromol.*, 2025, 140086.
  - 54 S. Farsad, A. Amjlef, A. Chaoui, A. Ben Hamou, C. Hamma, M. Benafqir, A. Jada and N. El Alem, Harnessing a carbon-based material from food waste digestate for dye adsorption: the role of hydrogel beads in enhancing the material stability and regenerative capacity, *Mater. Adv.*, 2023, **4**, 6599–6611.
  - 55 H. Es-Sahbany, R. Hsissou, M. L. El Hachimi, M. Allaoui, S. Nkhili and M. S. Elyoubi, Investigation of the adsorption of heavy metals (Cu, Co, Ni and Pb) in treatment synthetic wastewater using natural clay as a potential adsorbent (Sale-Morocco), *Mater. Today: Proc.*, 2021, **45**, 7290–7298.
  - 56 A. Amjlef, S. Khrach, A. Ait El Fakir, S. Farsad, S. Et-Taleb and N. El Alem, Adsorptive properties investigation of natural sand as adsorbent for methylene blue removal from contaminated water, *Nanotechnol. Environ. Eng.*, 2021, **6**, 26.
  - 57 A. Alanazi, H. R. Abid, I. S. Abu-Mahfouz, S. A. Bawazeer, T. Matamba, A. Keshavarz, S. Iglauer and H. Hoteit, Hydrogen adsorption kinetics in organic-rich shale reservoir rocks for seasonal geological storage, *Fuel*, 2025, **379**, 132964.
  - 58 S. Tripathy, S. Sahu, R. K. Patel, R. B. Panda and P. K. Kar, Efficient removal of  $\text{Cr}(\text{VI})$  by polyaniline modified biochar from date (*Phoenix dactylifera*) seed, *Groundw. Sustain. Dev.*, 2021, **15**, 100653.
  - 59 B. Abbou, I. Lebdiri and H. Ouaddari, Evaluation of Illitic-Kaolinite clay as an adsorbent for  $\text{Cr}^{3+}$  removal from synthetic aqueous solutions: Isotherm, kinetic, and thermodynamic analyses, *Chem. Phys. Impact*, 2024, **8**, 100527.
  - 60 S. Show, S. Mukherjee, M. S. Devi, B. Karmakar and G. Halder, Linear and non-linear analysis of Ibuprofen riddance efficacy by Terminalia catappa active biochar: equilibrium, kinetics, safe disposal, reusability and cost estimation, *Process Saf. Environ. Prot.*, 2021, **147**, 942–964.
  - 61 A. A. Adeyemo, I. O. Adeoye and O. S. Bello, Adsorption of dyes using different types of clay: a review, *Appl. Water Sci.*, 2017, **7**, 543–568.
  - 62 K. R. Hall, L. C. Eagleton, A. Acrivos and T. Vermeulen, Pore and solid-diffusion kinetics in fixed-bed adsorption under constant-pattern conditions, *Ind. Eng. Chem. Fundam.*, 1966, **5**, 212–223.
  - 63 M. Gouamid, M. R. Ouahrani and M. B. Bensaci, Adsorption equilibrium, kinetics and thermodynamics of methylene blue from aqueous solutions using date palm leaves, *Energy Procedia*, 2013, **36**, 898–907.





- 64 V. C. Silva, M. E. B. Araújo, A. M. Rodrigues, M. do, B. C. Vitorino, J. M. Cartaxo, R. R. Menezes and G. A. Neves, Adsorption behavior of crystal violet and congo red dyes on heat-treated brazilian palygorskite: Kinetic, isothermal and thermodynamic studies, *Materials*, 2021, **14**, 5688.
- 65 Y. Raji, A. Nadi, I. Mechnou, M. Saadouni, O. Cherkaoui and S. Zyade, High adsorption capacities of crystal violet dye by low-cost activated carbon prepared from Moroccan Moringa oleifera wastes: Characterization, adsorption and mechanism study, *Diamond Relat. Mater.*, 2023, **135**, 109834.
- 66 Z. Ahamad and A. Nasar, Polypyrrole-decorated bentonite magnetic nanocomposite: A green approach for adsorption of anionic methyl orange and cationic crystal violet dyes from contaminated water, *Environ. Res.*, 2024, **247**, 118193.
- 67 M. Yilmazoglu, N. Kanmaz and P. Demircivi, Constructing the synergistic effects of chitosan and ionic liquid on SPEEK polymer for efficient adsorption of crystal violet dye, *Int. J. Biol. Macromol.*, 2024, 132638.
- 68 R. Elmoubarki, F. Z. Mahjoubi, H. Tounsadi, J. Moustadraf, M. Abdennouri, A. Zouhri, A. El Albani and N. Barka, Adsorption of textile dyes on raw and decanted Moroccan clays: kinetics, equilibrium and thermodynamics, *Water Resour. Ind.*, 2015, **9**, 16–29.
- 69 O. S. Omer, M. A. Hussein, B. H. M. Hussein and A. Mgaidi, Adsorption thermodynamics of cationic dyes (methylene blue and crystal violet) to a natural clay mineral from aqueous solution between 293.15 and 323.15 K, *Arabian J. Chem.*, 2018, **11**, 615–623.
- 70 N. M. Mahmoodi, B. Hayati and M. Arami, Kinetic, equilibrium and thermodynamic studies of ternary system dye removal using a biopolymer, *Ind. Crops Prod.*, 2012, **35**, 295–301.
- 71 S. Choudhary, K. Sharma, V. Kumar and V. Sharma, RSM-CCD directed modeling and optimization of a low-cost adsorbent based on sodium dodecyl sulfate for the selective removal of malachite green and methylene blue dyes: kinetics, isotherm, and thermodynamics analysis, *Microchem. J.*, 2024, **205**, 111158.
- 72 H. Najafi, N. Asasian-Kolur and S. Sharifian, Adsorption of chromium(vi) and crystal violet onto granular biopolymer-silica pillared clay composites from aqueous solutions, *J. Mol. Liq.*, 2021, **344**, 117822.
- 73 S. H. Vithalkar and R. M. Jugade, Adsorptive removal of crystal violet from aqueous solution by cross-linked chitosan coated bentonite, *Mater. Today: Proc.*, 2020, **29**, 1025–1032.
- 74 S. Mohammad and I. Suzylawati, Study of the adsorption/desorption of MB dye solution using bentonite adsorbent coating, *J. Water Process Eng.*, 2020, **34**, 101155.
- 75 Z. Liang, Z. Zhao, T. Sun, W. Shi and F. Cui, Enhanced adsorption of the cationic dyes in the spherical CuO/mesoporous silica nano composite and impact of solution chemistry, *J. Colloid Interface Sci.*, 2017, **485**, 192–200.
- 76 A. Chaoui, S. Farsad, A. Ben Hamou, A. Amjlef, N. Nouj, M. Ezzahery and N. El Alem, Reshaping environmental sustainability: Poultry by-products digestate valorization for enhanced biochar performance in methylene blue removal, *J. Environ. Manage.*, 2024, **351**, 119870.
- 77 L. Zhang, H. Zhang, W. Guo and Y. Tian, Removal of malachite green and crystal violet cationic dyes from aqueous solution using activated sintering process red mud, *Appl. Clay Sci.*, 2014, **93**, 85–93.
- 78 J. Liu, H. Jia, Z. Xu, T. Wang, M. Mei, S. Chen, J. Li and W. Zhang, An impressive pristine biochar from food waste digestate for arsenic (v) removal from water: Performance, optimization, and mechanism, *Bioresour. Technol.*, 2023, **387**, 129586.
- 79 W. Ma, X. Song, Y. Pan, Z. Cheng, G. Xin, B. Wang and X. Wang, Adsorption behavior of crystal violet onto opal and reuse feasibility of opal-dye sludge for binding heavy metals from aqueous solutions, *Chem. Eng. J.*, 2012, **193**, 381–390.

